Journal of Imaging Science and Technology® 55(4): 040301-1–040301-6, 2011.

Ink Jet Technology for Large Area Organic Light-Emitting Diode and Organic Photovoltaic Applications

Maosheng Ren, Harrie Gorter, Jasper Michels, and Ronn Andriessen
Holst Centre/TNO, High Tech Campus 31, P.O. Box 8550, 5605 KN Eindhoven, The Netherlands
E-mail: mao.ren@tno.nl

Abstract. *Due to its flexibility and ease of patterning, ink jet printing has become a popular technique for the noncontact deposition of liquids, solutions, and melts on a variety of substrates at lateral resolutions down to 10 μm. This article presents a study of ink jet printing of homogeneous layers of Orgacon™ (Agfa-Gevaert, Belgium), a water-based dispersion of poly(3,4-ethylenedioxythiophene):poly (styrenesulfonic acid) (PEDOT:PSS). The printed PEDOT:PSS layer can be used as a transparent electrode in organic light-emitting diodes (OLEDs). Fundamental aspects of the interaction between the ink jet ink and the substrate and the resulting homogeneity of the active layer in relation to OLED device performance are investigated. The optimized PEDOT:PSS ink formulation is shown to improve layer homogeneity, resulting in a uniform light output and device efficiency. Ink jet printing is shown to be capable of fabricating 25 × 25 mm OLED devices that have equivalent efficiency and light uniformity to the ones produced by spin coating. © 2011 Society for Imaging Science and Technology.*
[DOI: 10.2352/J.ImagingSci.Technol.2011.55.4.040301]

INTRODUCTION

Organic light-emitting diodes (OLEDs) offer many benefits over traditional lighting technologies such as fluorescent tubes. However, for OLEDs to be widely adopted in commercial lighting applications, they need to have a comparable cost of ownership to traditional technologies.

Today, high efficiency white OLEDs are manufactured through the vacuum deposition of small molecules on glass substrates coated with a transparent conductive oxide such as indium tin oxide (ITO). However, vacuum processing is expensive for high volume, low cost OLED production, and roll-to-roll (R2R) deposition at atmospheric pressure is more appealing. Over the last decade, there has been an intensive search for cost-effective polymer light-emitting diodes (PLEDs) suitable for such production techniques.

As an alternative to vacuum techniques, wet solution deposition can provide significant cost savings by enabling R2R printing of large-area electronics on flexible substrates at low fabrication costs. Therefore, we are currently investigating high volume, R2R-compatible, solution-based deposition techniques.[1,2] A major topic in this research is ink jet printing of organic inks for printed electronics. This has the advantage of being a noncontact technique that offers an ease of patterning in various industrial processes. For high accuracy deposition of (low viscosity) functional material solutions at specific locations on a substrate, ink jet technology enables fast and easy deposition of thin polymer films over large areas.

Furthermore, the past few years have seen the development of reliable and robust ink jet printer heads, making ink jet technology more mature for single-pass document and graphics production.[3] This development opens new opportunities for using industrial ink jet technology in manufacturing printed electronics including PLEDs[4,5] and thin film transistors.[6,7] Ink jet printing has been used to fabricate polymer:fullerene bulk heterojunction organic photovoltaics (OPVs). Here, the OPV cell is made from an active layer of poly(3-hexylthiophene) (P3HT) and [6,6]-phenyl C_{61}-butyric acid methyl ester (PCBM) blends.[8,9]

The replacement of the ITO layer by a printable transparent electrode and metal structures on a thin-film encapsulated flexible OLED has previously been demonstrated using spin coating.[10] Currently, poly(3,4-ethylenedioxythiophene) doped with poly(4-styrenesulfonate) (PEDOT:PSS) is used as a transparent electrode for the OLEDs. Furthermore, in combination with printed silver nanoparticles, OLED devices have been demonstrated.[11]

This article will demonstrate the use of ink jet technology in the fabrication of flexible OLEDs. The main challenge in using ink jet technology is the deposition of highly homogenous layers of active materials onto flexible substrates. As a benchmark, device performance will be compared with spin-coated reference devices.

Moreover, several process requirements for the deposition of homogeneous electroactive layers will be investigated. These include substrate pretreatment to modify the surface energy and ink formulations to yield stable ink jet inks with concentration, wetting behavior, and rheological behavior determined by the boundary conditions for a robust deposition process. Furthermore, we will demonstrate uniform light output of OLED devices on foils with a moisture barrier.

With sufficient reproducibility and reliability, the processing techniques may be applied not only to the fabrication of flexible OLED lighting but also for systematic moisture barrier analysis of thin-film encapsulated foil-based OPVs.

Received Dec. 9, 2010; accepted for publication Apr. 25, 2011; published online Jul. 28, 2011
1062-3701/2011/55(4)/040301/6/$20.00.

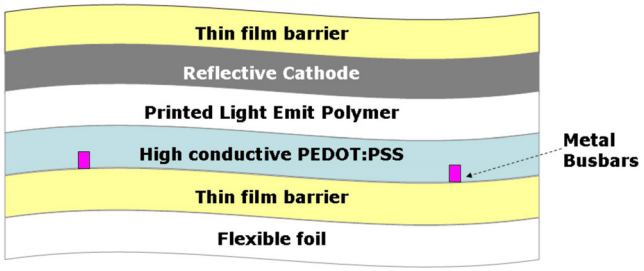

Figure 1. Schematic representation of a bottom-emitting (ITO-free) OLED on foil.

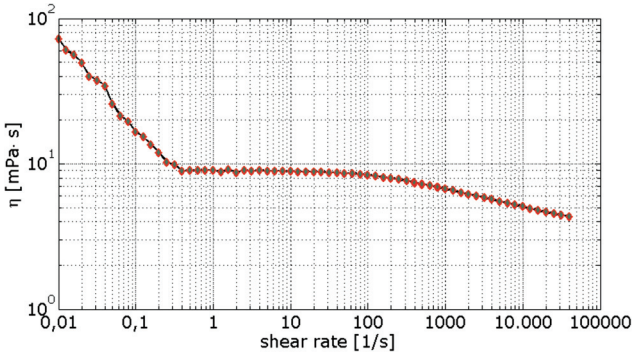

Figure 2. PEDOT:PSS ink viscosity as function of shear rate, measured with an Anton Paar Physica MCR rheometer.

EXPERIMENTAL

Device Stacks

OLEDs were fabricated on a 150 × 150 mm Teonex® PEN foil from Dupont Teijin Films, onto which a silicon nitride-based moisture barrier was applied. This transparent barrier was created through low-temperature plasma deposition of amorphous hydrogenated silicon nitride films and was stacked with planarization layers to spatially separate defects. To further limit the ingress of water and oxygen, the same barrier was also applied as an encapsulation stack on top of the manufactured OLEDs, as sketched in Figure 1.

Our glass-based (ITO-free) OLED device typically consists of a transparent anode, a hole-injection layer (PEDOT:PSS), a white-light-emitting polymer (LEP, Merck Livilux™) and barium (5 nm)/aluminum (100 nm) as the cathode. A highly conductive PEDOT:PSS layer (Agfa Orgacon™ ILHC5 IJ) served simultaneously as the transparent anode and as the hole-injection layer.

The OPV device stack is very similar to the OLED stack. However, instead of a light-emitting polymer, a P3HT/PCBM donor-acceptor blend is deposited on top of the PEDOT:PSS layer and covered with LiF/Al as a reflective cathode.

Metal busbars/lines around or within the active area can be deposited by printed metals. The metal structure within the active area either was honeycomb shaped or consisted of one or more (evenly spaced) lines. Dry layer thicknesses were typically 100 nm for the highly conductive PEDOT:PSS and 200 nm for the P3HT/PCBM blends.

Equipment

Deposition was carried out using a piezoelectrically actuated Spectra Galaxy PH 256/50 AAA ink jet printer head. The nozzle pitch was 254 μm, while the drop volume (V_{drop}) and drop ejection frequency (f_{drop}) were kept constant at 50 pl and 1 kHz, respectively. The lateral separation of neighboring printed lines could be varied by adjusting the azimuthal orientation of the printer head with respect to the direction of substrate motion.

For the OLEDs, current–voltage–light (IVL) characteristics were measured using a Keithley 2400 general-purpose source meter. During the IVL cycle, the brightness was monitored by a photodiode calibrated with a Konica Minolta LS-100 luminance meter. The luminance meter was mounted orthogonally to the OLED, which was connected to a Keithley 6517A electrometer/high-resistance meter. The systematic error in these measurements is estimated to be ±10%.

The current density–voltage (JV) characteristics of the OPV devices were measured using simulated air mass filter (AM) 1.5 global solar irradiation (100 mW/cm^2). The light source was a xenon-lamp solar simulator, which was calibrated with a standard silicon photodiode detector.

Materials

For experiments and device fabrication, a commercially available dispersion of 1 wt. % PEDOT:PSS (Orgacon™ HILHC5-IJ, Agfa Gevaert N.V.) in water was used. PEDOT:PSS is basically a (99%) water-based polymer dispersion.

RESULTS AND DISCUSSION

Ink Rheology

Figure 2 shows the measured PEDOT:PSS ink viscosity as a function of shear rate (measured with an Anton Paar Physica MCR rheometer). For shear rates >1 s^{-1}, the ink exhibits near-Newtonian flow, with slight shear thinning behavior. Maximum shear rates for most ink jet heads are of the order 10^5–10^6 s^{-1}. Depending on molecular weight and shear rate, the PEDOT:PSS droplet formation shows viscoelastic behavior.

To obtain a stable droplet formation without satellites and short ligaments, the solution concentration and the drop formation waveform must be optimized for the ink jet printer head used. The surface tension of the ink will significantly influence the droplet formation as well.

The high surface tension of water causes poor wetting of the substrate. Hence, surfactants were added to reduce surface tension and improve wetting behavior, as shown in Figure 3. Depending on the surfactant additives used, the equilibrium surface tension of the PEDOT:PSS dispersion was in the range $\gamma = 25$–40 mN/m.

Wetting properties are also influenced by the surface energy of the substrate. For an OLED device, it is common for the substrate to be structured with silicon nitride and

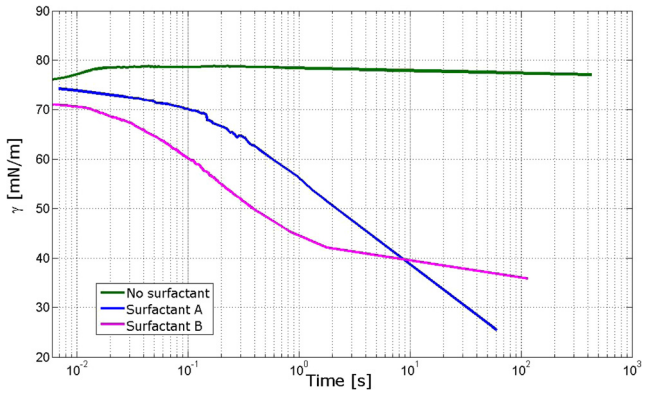

Figure 3. Effect of surfactant, measured surface tension as function of time.

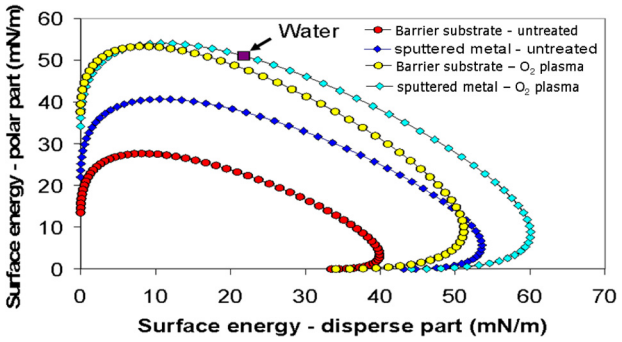

Figure 4. Wetting envelopes for untreated and pretreated substrates.

metal busbars/lines. Wetting behavior is different for each substrate material.

Figure 4 shows wetting envelopes for each substrate material. The polar and disperse coordinates of water, the main component of PEDOT:PSS inks, show the relation between the ink and the substrate. If the surface energy of the substrate is much lower than the surface tension of the ink—as is the case for the untreated substrates—wetting, spreading, and layer formation will be poor. Large differences in the surface energy between ink and substrate will cause inhomogeneous layer formation or even dewetting spots. Plasma treatment can be used to increase the surface energies of the substrate and sputtered metal, both substrate materials, and reduce the difference between them, as shown in Fig. 4. This allows layer formation to be controlled.

Droplet Spreading and Coalescence

To model the ink jet printing process, we assume that the printer head produces ink droplets of a uniform volume (V_{drop}) and diameter (D_{drop}) at a constant jetting frequency f_{drop}. These droplets hit a nonporous substrate, which moves at a constant speed (U_{sub}). After impact, the drop takes on a spherical cap shape of diameter D_{cap}. The drops coalesce to form a line of width w. This picture of ink jet printing is represented graphically in Figure 5.

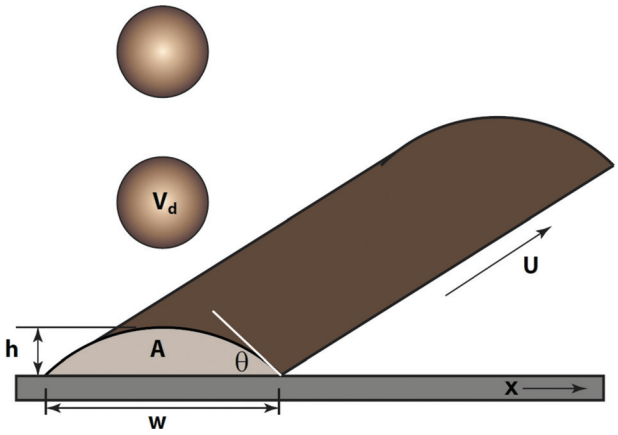

Figure 5. Definition of ink jet droplet impact on a nonporous substrate to form a single line.

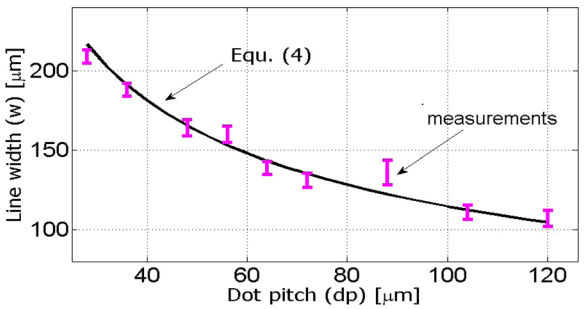

Figure 6. Line width of printed PEDOT:PSS as function of dot pitch, comparison between experimental measurements and theoretical predicted values.

For narrow single lines, i.e., where $w << \ell_c \equiv \sqrt{\gamma/(\rho g)}$; ℓ_c is the capillary length (a material parameter), γ is the surface tension of the ink, ρ is the fluid density and g is gravitational acceleration, the line width can be calculated to be

$$w = 2\sin\theta_e \sqrt{\frac{A}{(\theta_e - \sin\theta_e \cos\theta_e)}} \tag{1}$$

where A is the cross-sectional area (volume per unit length) of the printed line and θ_e is the equilibrium contact angle between the ink and the substrate.

The equilibrium contact angle is a constant for a given ink and substrate combination, depending on the properties of the two materials. However, in practice, measuring θ_e directly is nontrivial due to contact line hysteresis. Instead, for a given (homogeneous and preconditioned) substrate, it can be derived from the spreading ratio of the (measurable) diameters of the initial drop and the resulting cap on the substrate, which is given by

$$\text{SR} = \frac{D_{\text{cap}}}{D_{\text{drop}}} = \left[\frac{4\sin^3\theta_e}{(1-\cos\theta_e)^2(2+\cos\theta_e)}\right]^{1/3} \tag{2}$$

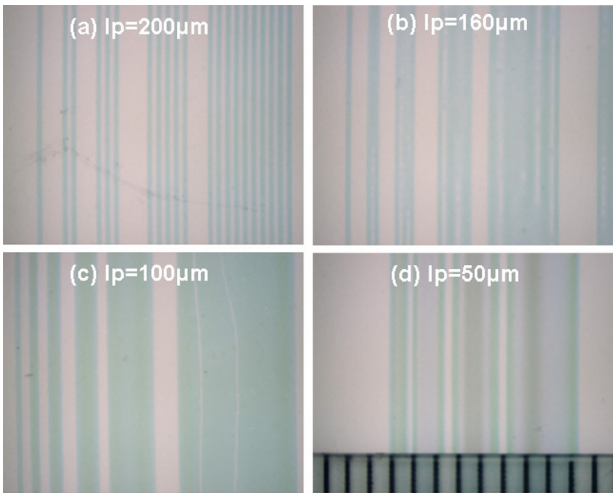

Figure 7. Ink jet-printed PEDOT:PSS stripes deposited with line pitches (L_p) of (a) 200 μm, (b) 160 μm, (c) 100 μm and (d) 50 μm. The white scratches in (c) are the result of Dektak scanning-probe measurements.

Alternatively, a close approximation θ_0 can be estimated by measuring the advancing and receding contact angles (θ_A and θ_R, respectively) and taking a trigonometric average:

$$\cos\theta_0 = \frac{(\cos\theta_A + \cos\theta_R)}{2} \tag{3}$$

To use Eq. (1), we also need to know the cross-sectional area of the line. In ink jet printing, this can be controlled by altering the substrate speed and jetting frequency and is defined by:

$$A = \frac{V_{\text{drop}}}{d_{\text{p}}} = V_{\text{drop}}\frac{f_{\text{drop}}}{U_{\text{sub}}} \tag{4}$$

where the quantity d_{p} is known as the droplet pitch. For narrow and thin single lines, i.e., if $h \ll w$, the cross-sectional profile is parabolic to a good approximation and h is the center height of a printed single line.

From Eqs. (1) and (4), we see that, for a given substrate and ink and a constant drop volume, the width of the printed line depends only on d_{p}. Figure 6 shows good agreement across a range of dot pitches between the results of this theoretical model and measured line widths of in PEDOT:PSS ink jet printed onto the moisture barrier used. The experimental measurements were obtained using a microscope image and Stylus profilometer.

In practice, at very low dot pitches, the cap of a line contains too much ink, leading to uncontrolled spreading. As known from previous work, wetting instability occurs if the dot pitch becomes too small.[12] A smooth line can be created by increasing the dot pitch. However, if the dot pitch becomes too large, capillary effects cause a regular pattern of wider and narrower parts in the line.[13] At even larger dot pitches, the drops will no longer merge into a continuous line.

Layer Formation

Figure 7 shows four series of ink jet-printed PEDOT:PSS lines of various line pitches that were deposited on a non-porous substrate (silicon nitride) with line pitches (L_p) between 50 and 200 μm. Generally, patterns were printed such that the center-to-center distance of neighboring lines was smaller than the line width, $L_p < w$, guaranteeing a certain minimum overlap. The width of a single line (w) was approximately 200 μm.

Moreover, d_{p} was kept much smaller than L_p, so that the leveling dynamics proceeded much faster in the printing direction (y-axis) than perpendicular to it. Hence, in this work, lateral leveling is only considered along the x-axis and the ink thickness profile, $h(x,y,t)$, is assumed to be independent of y. For industrial applications, it is desirable to maximize L_p and U_{sub} to allow larger areas to be printed faster and with fewer printer heads.

The grayscale contrast in the microscope images reflects the thickness profile of the printed stripes. Fig. 7(a) shows distinct individual lines that have not merged laterally at all. Fig. 7(b) clearly shows the onset of coalescence. The grayscale contrast in Fig. 7(c) is very uniform indicating near-optimal leveling. In Fig. 7(d), the very small line pitch resulted in a larger overall film thickness. The grayscale distribution indicates that the thickness profiles of the stripes are not flat but more closely resemble parabolas as a consequence of capillary redistribution.

Furthermore, we are developing a theoretical model of the leveling and redistribution dynamics of ink jet-printed

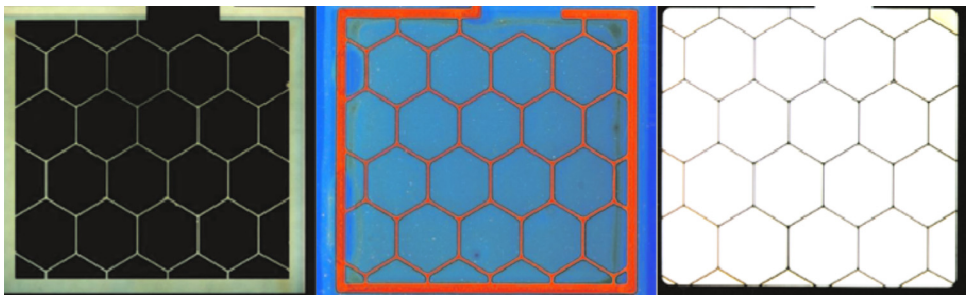

Figure 8. Photographs of (a) ink jet-printed PEDOT on a glass substrate with sputtered metal, (b) Livilux™ LEP ink jet printed over the PEDOT layer (under UV illumination) and (c) electroluminescence, after cathode evaporation and encapsulation with a metal lid, of the device when driven at a voltage of 8 V.

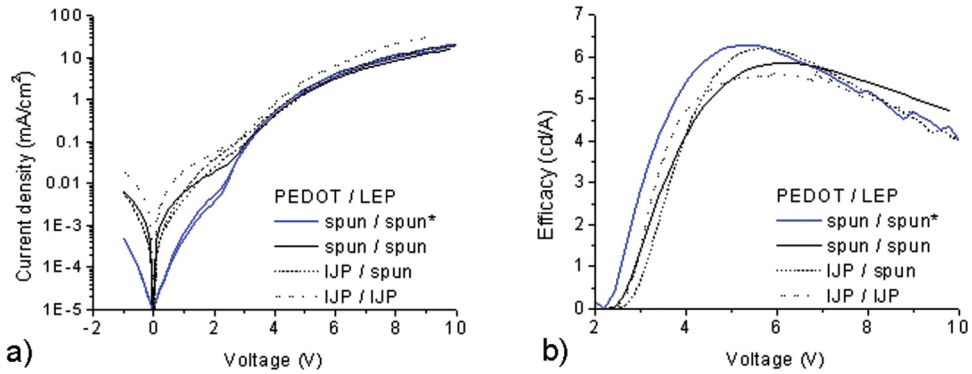

Figure 9. IVL measurement of 25 × 25 mm OLEDs on glass with benchmark of spin-coated and ink jet-printed HILHC5 PEDOT:PSS and LEP layers.

lines in the presence of surfactants. Both the fluid properties and printer parameters can influence the leveling rate and subsequently affect the equilibration dynamics of multiple ink jet-printed lines.[14] This simple model provides a basis for estimating ink jet process windows.

Characteristics of Printed OLEDs

As explained previously, our glass-based (ITO-free) OLED device typically consists of a transparent anode, a hole-injection layer (PEDOT:PSS), a white-LEP (Merck Livilux™) and barium (5 nm)/aluminum (100 nm) as the cathode. Metal busbars around and within the active area were created in a honeycomb pattern through screen printing or RF patterning. These structures were 1.5 μm high when screen printed and 300 nm high when sputtered. In both case, the metal lines were of the order of 200 μm wide.

The PEDOT:PSS and the LEP were deposited from solution using ink jet printing under ambient conditions. Typical dry layer thicknesses were 100 nm for the PEDOT:PSS and 80 nm for the LEP. After thermal evaporation of the cathode, the devices were sealed by applying a metal lid with an ultra-violet curable epoxy adhesive.

Figure 8 shows photographic images of the ink jet-printed OLED at various stages of production: after ink jet printing the PEDOT:PSS layer, after ink jet printing the LEP (on top of the PEDOT:PSS) and the finished device driven at 8 V. Fig. 8(c) shows that the light output of the ink jet-printed OLED is extremely uniform.

Figure 9 compares the IVL performance of four 25 × 25 mm OLEDs produced using various combinations of ink jet printing and spin coating for the PEDOT:PSS and LEP layers. All PEDOT:PSS layers were formed from the same Orgacon ink jet printing formulation. The exception was a benchmark OLED created using spin coating and indicated in blue on the graph.

In general, the IVL cycles of the four nearly overlap. The OLED with the ink jet-printed LEP layer does exhibit a somewhat higher IV profile, stemming from local layer thickness variations. In addition, the parasitic current in the low-voltage regime before turn-on is higher than for spin-coated samples. These leakage currents could be due

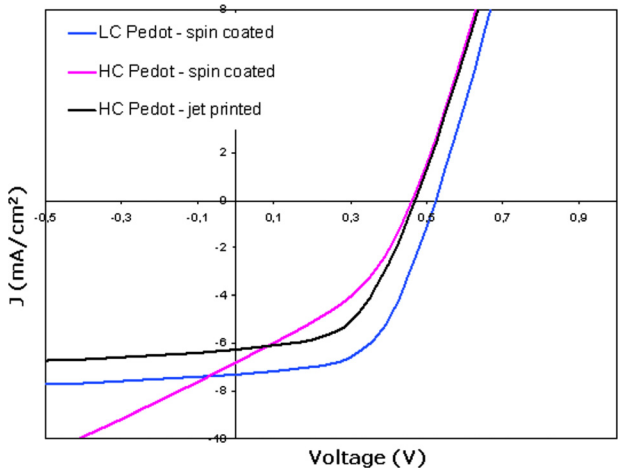

Figure 10. Device performance of 25 × 25 mmOPV on glass with benchmark of spin-coated and ink jet-printed PEDOT:PSS and spin-coated OPV layers.

to dust, scratches, etc., in the active area. Alternatively, they could be due to inhomogeneity in the LEP layer (the use of high-conductivity PEDOT:PSS requires extremely homogeneous LEP coverage).

Deposition of the LEP by ink jet printing again poses a challenge: namely, forming a homogeneous film on a hygroscopic PEDOT:PSS surface. Fig. 8 shows uniform light emission with optimal droplet formation, compatibility with the substrate, coalescence, leveling, and drying to form a homogeneous 80 nm dry LEP layer. Despite this complexity, the brightness and efficacy levels were found to be in the same range as the OLEDs manufactured by spin coating, as shown in Fig. 9.

Characteristics of Printed OPVs

Various PEDOT:PSS ink formulations (conductive variations) and deposition techniques (spin coating versus ink jet printing) have been investigated. The device performance of a 25 × 25 mm OPV cell has been measured, as shown in Figure 10.

Ink jet printing PEDOT:PSS delivers layer homogeneity and device performance that is comparable with spin

coating. When using the same PEDOT:PSS formulation, the ink jet-printed OPV device shows slightly better performance in terms of leakage current than the spin-coated version. This might be related to the removal procedure for spin-coated PEDOT:PSS film. Such a step is not required for ink jet-printed devices, which could have potential benefits for upscaling of R2R OPV production.

CONCLUSIONS

In this work, some fundamental aspects of the interaction between ink jet ink and substrate have been addressed. The resulting homogeneity of the active layer (PEDOT:PSS) and related device performance of OLED and OPV have been investigated.

PEDOT:PSS and a LEP were deposited in homogeneous layers using commercially available printer heads. Using a combination of theoretical and experimental approaches, the ink jet formation and creation of homogenous layers on a moisture barrier was optimized. Furthermore, the ability to use ink jet printing to fabricate 25×25 mm OLED devices has been demonstrated.

Ink properties and substrate pretreatments have also been optimized to ensure robust printing and drying processes. The resulting ITO-free OLEDs on glass using ink jet-printed PEDOT:PSS and ink jet-printed LED layers were found to exhibit uniformity of light emission, and device performance comparable with spin-coated reference devices.

ACKNOWLEDGMENTS

Holst Centre is an open innovation research centre founded by TNO and IMEC that is developing roll-to-roll production techniques for foil-based organic electronics and wireless autonomous transducer solutions, in cooperation with industry and universities. This research is supported by the Dutch Ministry of Economic Affairs, Philips Research, Agfa-Gevaert N.V., and Merck KGaA. The authors would like to thank Martin Hack, Peter Kruijt, Jorgen Sweelssen, Nadia Grossiord, Julia Galagan, Juliane Gabel, Charlotte Kjellander, Eric Rubingh, Gerwin Kirchner, Stephan Harkema, Edward Young, and Ton van Mol for their help in preparing and measuring devices.

REFERENCES

[1] S. Harkema, M. Ren, J. S. Gabel, J. E. J. M. Rubingh, I. G. de Vries, H. A. J. M. Andriessen, and A. M. B. van Mol, *Proc. LOPE*-C (LOPE-C, Frankfurt, Germany, 2010).
[2] J. J. Michels, S. H. P. M. de Winter, and L. H. G. Symonds, Org. Electron. **10**, 1495 (2009).
[3] H. Wijshoff, Phys. Rep. **491**, 77 (2010)
[4] J. Stringer and B. Derby, J. Eur. Ceram. Soc. **29**, 913 (2008).
[5] E. Tekin, P. J. Smith, and U. S. Schubert, Soft Matter **4**, 703 (2008).
[6] H. Sirringhaus, T. Kawase, R. H. Friend, T. Shimoda, M. Inbasekaran, W. Wu, and E. P. Woo, Science **290**, 2123 (2000).
[7] M. Singh, H. M. Haverinen, P. Dhagat, and G. E. Jabbour, Adv. Mater. **22**, 673 (2010).
[8] C. N. Hoth, S. A. Choulis, P. Schilinsky, and C. J. Brabec, Adv. Mater. **19**, 3973 (2007).
[9] S. H. Eom, S. Senthilarasu, P. Uthirakumar, S. C. Yoon, J. Lim, C. Lee, H. S. Lim, J. Lee, and S. H. Lee, Org. Electron. **10**, 536 (2009).
[10] S. Harkema, S. Mennema, M. Barink, H. C. A. Rooms, J. S. Wilson, A. M. B. van Mol, and D. Bollen, Proc. SPIE **7415**, 74150T (2009).
[11] J. E. J. M. Rubingh, P. G. M. Kruijt, and H. A. J. M. Andriessen, *Proc. LOPE-C* (LOPE-C, Frankfurt, Germany, 2009).
[12] P. C. Duineveld, J. Fluid Mech. **477**, 175 (2003).
[13] D. Soltman and V. Subramanian, Langmuir **24**(5), 2224 (2008).
[14] M. Hanyak, A. A. Darhuber, and M. Ren, J. Appl. Phys. **109**, 7 (2011).